

Projector-Based Augmented Reality System for Interventional Visualization Inside MRI Scanners

PRE-PRINT version¹

André Mewes² Florian Heinrich² Urte Kägebein² Bennet Hensen³
Frank Wacker³ Christian Hansen²

August 24, 2018

Background Navigation support in the interventional MRI is separated from the operating field, which makes it difficult to interpret positions and orientations and to coordinate the necessary hand movements.

Methods We developed a projector-based augmented reality system to enable visual navigation of tracked instruments on pre-planned paths, and the visualization of risk structures directly on the patient inside the MRI bore. To assess the accuracy of the system a user study with clinicians was carried out in needle navigation test scenario.

Results The targets were reached with an error of 1.7 ± 0.5 mm, the entry points with an error of 1.7 ± 0.8 mm.

Conclusion The results suggest that the projected augmented reality navigation directly on the patient is accurate enough to target lesions with a size of down to 15 mm, so that prototype can serve as a platform for current and future research in augmented reality visualization and dynamic registration.

Keywords: Image-Guided Interventions, Augmented Reality, Magnet Resonance Imaging, Interventional Radiology

1 Introduction

In recent years, there has been a significant trend away from open surgery towards minimally-invasive therapies. It is proven that minimally-invasive interventions decrease the risk for the patient in terms of infections and damage to healthy tissue. As a result mortality rates are reduced and recovery time is shortened [1]. Because the patient's body is not opened for such treatments, radiological images are requisite to locate the target, surgical instruments, and surrounding risk structures.

¹**The final version contains some more references, a more comprehensive calibration section, more sophisticated discussion, and a comparison of the accuracy with state of the art methods.**

² Otto-von-Guericke-University Magdeburg, Faculty of Computer Science
Magdeburg, Germany
andre.mewes@ovgu.de

³ Hannover Medical School,
Institute of Diagnostic and Interventional Radiology

This is the reason why many needle-based interventions are nowadays carried out with the help of ultrasound (US) or CT scanners [2, 3]. Although US is compact, cheap and widely available, deep structures within the body especially under bones are hardly visible [4, 5, 6]. In contrast, CT enables an appropriate representation of the whole operating area. However, it uses harming ionizing radiation and has only a limited soft tissue contrast [7]. MRI instead does not emit ionizing radiation and is characterized by an excellent soft-tissue contrast. Target lesions can be identified, which cannot be seen on either US or CT. Besides that, a variety of instrument tracking is enabled through the possibility of acquiring imaging planes in oblique orientations [6, 8]. Additionally, morphologic as well as functional information (e.g. temperature changes, blood flow, and diffusion) can be monitored. Thus, MRI represents a unique approach to diagnose and treat diseases within minimally-invasive procedures [9]. However, interventional MRI (iMRI) is mainly limited to few clinical centers due to access and workflow limitations [10]. In order to make iMRI a standard interventional procedure, the development of an appropriate guidance support is essential to simplify and shorten the intervention. Such assistance is used frequently and often presented on a dedicated display outside the MRI which separates it from the operation field increasing mental load [11]. It is difficult to accurately interpret the guidance of tools to a specific position, orientation, and depth when presented on an external monitor [12]. Therefore, it is advantageous to fuse the separate virtual data directly in the operating field in terms of augmented reality (AR).

Medical AR for MRI-guided Interventions

The first augmented reality (AR)-based needle guidance system for use with MRI is described by Gering et al. [13]. The system is based on an MR conditional monitor that is located inside an open 1.5 T MRI (double-donut configuration). It does not provide a spatial AR environment because the virtual information is visualized separately from the patient. Wacker et al. [14] augmented the radiologist’s view of the patient with 2D anatomical images and a virtual needle for needle biopsy guidance, using a head-mounted display (HMD) and tracked instruments (optical see-through AR). However, due to the strong magnetic field of the MRI scanner, the patient has to be translated out of the MRI for the HMD to work and also to not endanger the physician. An optical see-through system based on a transparent mirror presented in [15] was revised by Weiss et al. [16] to make it work inside the MRI scanner room. It was successfully tested by U-Thainual et al. [17] for preclinical use and by Fritz et al. [18] for applicability during lumbar spine procedures. The mirror is located above the table outside the MRI scanner. A 2D anatomical image centered on the current needle position is aligned with the patient and overlaid on the mirror. Due to the size of the equipment this system cannot be used inside the MRI bore, so the patient has to be moved out of the scanner to perform the needle puncture.

As the workspace is very limited and the use of materials is restricted due to the strong magnetic field, large and/or MR unsafe devices such as HMDs, monitors, or mirrors in front of the physician cannot be used in-bore, nor can a mobile projector proposed in [19, 20, 21]. In this paper, we present the first projector-based AR system to provide an accurate, reliable visualization directly in the operation field inside an MRI scanner. Another interventional projector-based AR approach has been explored in the field of gastrointestinal, hepatobiliary and pancreatic surgery by Sugimoto et al. [22], and for use in neurosurgery by Besharati Tabrizi et al. [23], who also use projected visualizations to augment the surgeon’s view of the scene with anatomical data.

Our spatial AR system is used to visualize arbitrary 3D planning data in correct perspective and alignment in the operation field and serves as a platform for further development of interventional AR visualization and interaction techniques. Our aim is to provide a multi-purpose AR system for in-bore interventions. To this end, we set up a

needle navigation test scenario with a tracked needle and navigation clues.

2 Materials and Methods

To realize a spatial AR environment with a projection inside an MRI scanner, align image data to the patient or phantom, and visualize it in the operating area, the following steps are necessary:

- Hardware Setup
 - Placing the projector and adjusting zoom and focus.
 - Positioning a camera to view the whole projection area.
- Calibration Process
 - Calibrating the projector with the camera.
 - Calibrating the MRI scanner with the projector-camera system.
- Data acquisition
 - Generating a virtual point cloud representation of the projection surface with a structured light approach.
 - Generating an anatomical patient dataset with the MRI.
 - Segmenting and meshing the structures of interest.
- Visualization
 - Determining correspondence between 3D points of the surface point cloud and the world coordinates of the projector’s pixel positions.
 - Projecting 3D patient data and navigation clues physically aligned and perspective-correct.

These steps are described in detail hereinafter.

Hardware Setup

An NEC PX700W Digital Light Processing ultra-long-throw projector (NEC Display Solutions Europe GmbH, Munich, Germany) at a resolution of 1024×768 px is placed outside a Siemens MAGNETOM Skyra 3T MRI (Siemens Healthcare AG, Munich, Germany) along the z-axis (head-feet) of the MRI scanner device. The light is guided through a waveguide and three mirrors onto the patient (see Fig. 1). In principle, a higher resolution could be used, but the projector’s optics and the size of the mirrors are limiting factors.

This resulted in a projection distance of 3.5 m and a real image size of 35×47 cm (width by height). Due to the requirement that as little space as possible should be used for the projection system, the mirror inside the bore is mounted horizontally. This leads to a small incidence angle so that the image is stretched in the height dimension. The built-in keystone correction is not applied, since the undermentioned calibration algorithm calculates coefficients for all occurring distortions. Otherwise, the stereo calibration would be corrupt due to false projector intrinsics.

For this to be achieved, a Qumox SJ4000 wide-angle camera (Qumox, Kowloon Bay, Hongkong) with a 170° opening angle was placed inside the MRI bore above the projection zone and along the z-axis. In this position, there is only an infinitesimal force applied to the camera body, and the whole projection area can be observed at a resolution of 1280×720 px with 30 frames per second from a distance of 20 to 47 cm. The chosen camera is not an MR-safe model; this will be addressed in future experiments. With this setup the

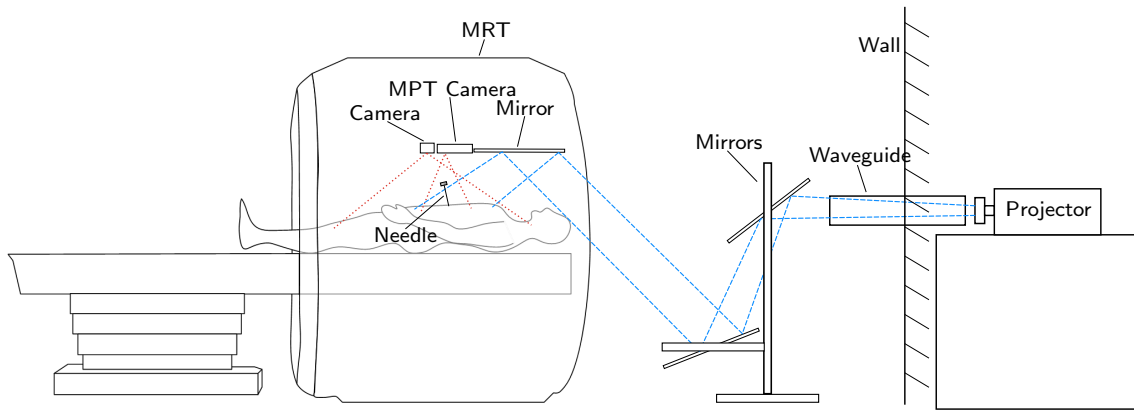


Figure 1: Schematic drawing of the complete hardware setup.

MR image quality is not influenced in such a manner that the user study described below could have been disturbed. The camera’s exposure value needs to be increased to EV +1 and the film speed set to ISO 100 to remove the rainbow effect caused by the projector’s rotating color wheel.

For the setup of the needle navigation test scenario, an MRI-compatible tracking camera (Metria Innovation, Inc., Wauwatosa, WI, USA) is mounted inside the bore, next to the mirror and wide-angle camera, to track moiré phase markers attached to the needle instrument. The pose of the markers can be obtained with a position error of less than 1 mm at a distance of 2.5 m and an orientation error of 0.05° . The camera’s tracking rate is between 1 and 15 FPS, depending on the distance: the nearer the tracked markers, the slower the marker recognition.

Calibration Process

The projector is calibrated with the structured-light approach proposed by Moreno et al. [24]. Here, 22 grey code patterns are projected onto a chessboard with defined size (see Fig. 2), and local homographies, i.e. transforms between the calibration points projected onto the chessboard and those observed by the camera, are calculated. In this manner correspondence between pixels and world coordinates is determined. The projector and the camera are calibrated as two separate cameras with the help of OpenCV¹. We adapted the projector calibration approach of [24] to use parameters from a separate camera calibration that uses a ChArUco board [25, 26] instead of an ordinary chessboard. These boards have more distinguishable features that can be used to interpolate between corner points, which results in a more accurate calibration. Due to the interpolation of markers and corners, they are also very robust against partial occlusion of the board. The stereo calibration provided the world coordinate transform between camera and projector. Six sets of grey code patterns on the chessboard – each in a different orientation – are used for the projector calibration. This calibration step has only to be performed initially or when the projector, camera, or mirrors have been moved.

In order to be able to project the anatomical patient data onto the real patient, the projector-camera system has to be registered with the MRI. A calibration body was printed and filled with transparent liquid candle wax (paraffin, Vaseline, white oils, see Fig. 4), which provides a clear contrast in a T1 sequence and causes little noise. The parallelism of the body’s edges in the corresponding MR dataset is best ensured by the MRI scanner’s built-in 3D distortion correction. A ChArUco board is attached on top of the plane surface of the calibration phantom so that it is aligned parallel with the candle wax. The pose of the

¹<http://opencv.org/>

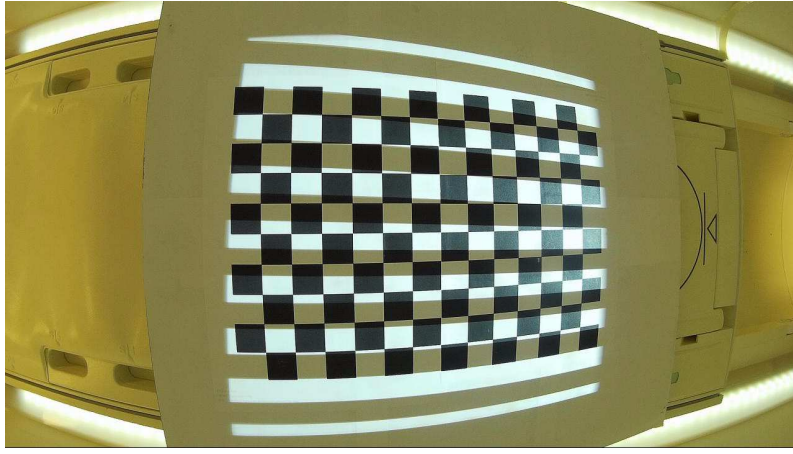


Figure 2: One of the projected grey code patterns on the chessboard during projector calibration from the view of the wide-angle camera.



Figure 3: Estimation of the fixed ChArUco marker pose for registration of the MRI coordinate system with the camera coordinate system.

board is estimated with the OpenCV function `cv::aruco::estimatePoseCharucoBoard()` [25] with the previously calibrated camera.

The calibration body's 3D corner points in the camera coordinate system are calculated from the known dimensions of the candle wax body (without the printed case, i.e. $115 \times 115 \times 117.5$ mm) and the axis parallel ChArUco marker pose. The corresponding points in patient coordinates are then measured in the DICOM dataset of the calibration body. The transform between the corner points in the camera coordinate system and the MRI coordinate system was estimated by the RANSAC-based `cv::estimateAffine3D()` from the OpenCV toolkit with a confidence of 0.99. For persistence of this rather elaborate calibration, a ChArUco marker is fixed to the bottom of the MRI bore (see Fig. 3), for which the transform to the MRI coordinate system is calculated and saved to a calibration file. Thus, only the projector calibration needs to be repeated when the camera, projector or mirrors are moved.

Finally, the moiré-phase tracking (MPT) tracking system, the needle, and the wide-angle camera need to be calibrated. Four moiré markers were attached to a needle and calibrated with a tracked calibration body. The preexisting cross-calibration between the moiré tracking system and the MRI is read from a calibration file. The MPT tracking system and the wide-angle camera share the MRI as a common coordinate system, which is used for determining the transform. This one-time calibration step takes approximately 30 min



Figure 4: Calibration body filled with candle wax for MRI imaging and with a ChArUco board attached to estimate the phantom's pose in camera coordinates.

under the condition that the hardware is already in place.

Data Acquisition and Visualization

As a test setup, a needle navigation application in the abdomen is realized. Before anatomical data and navigation clues can be projected onto the patient or phantom, the projection surface needs to be transferred into a dense point cloud via the structured light method provided by Moreno et al. [24]. This point cloud is manually filtered, resampled, and cleared of outliers. From the filtered point cloud a mesh is generated.

The acquired data then needs to be processed to render information on the phantom surface. First, the projection surface point cloud is used to determine which projector pixel correlates to which 3D world coordinate of the surface. In the process, each point is projected to its two-dimensional position in pixel coordinates using the projection matrix of the projector derived from the calibration step. Because of the low density of the point cloud compared to the dense pixel structure, not every pixel position is represented by a known world point. The gaps are filled through interpolation.

Next, a ray casting is performed to determine which structures are visible from a certain point of view and to determine where to draw them. For each projection pixel, a ray originating at the user's point of view and pointing towards the pixel's respective world coordinate is checked for intersection with world objects. Because a fixed viewing position is assumed for now, some static structures only need to be processed once while other dynamic structures need to be processed frequently. The calculated depth values for all objects are then combined to generate the projection image. The visualization includes risk structures derived from the MRI scan, a target for the needle-based intervention, the part of the needle that is inside the body, and a virtual extension of that needle. Risk structures, such as blood vessels, and other anatomical parts, e.g. ribs, are rendered transparently to avoid occlusion.

In addition, the rendering of the three-dimensional scene is augmented by needle navigation clues. These clues include a circle to indicate where the needle should be inserted (entry point), a depth-encoded virtual needle that shows the current needle orientation under the surface for the purpose of aiming at the target, and a circle to indicate where

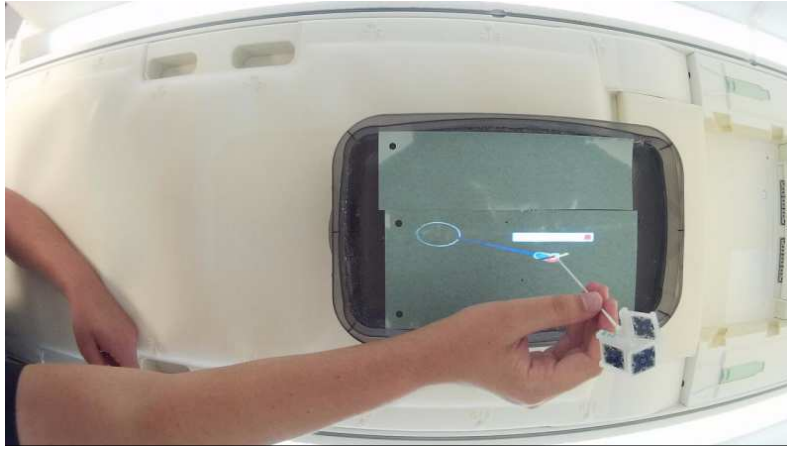


Figure 5: View of the projected scene from above with the wide-angle camera. Red is the insertion point, blue is the needle under the surface, and the faint green circle with the white contour is the target. The thickness and color of the virtual needle indicate depth.

the (virtual) needle intersects the projection surface. The target consists of an outer and an inner circle that change the color from slightly red to a faint green when hit by the virtual needle, indicating the correct orientation. When hit by the real needle, the target is strongly green colored to confirm successful insertion into the target.

3 Evaluation

The main issue of the evaluation was the assessment of the accuracy of the AR system. First, the reprojection errors of camera, projector, and stereo calibration from five different calibration procedures were determined. Second, the pose statistics of the ChArUco markers were calculated for 100 pose estimations to evaluate repetition accuracy. In order to evaluate the accuracy of the projected AR contents, we had eight different participants simulate a needle insertion using the needle guidance described above: four radiologists with more than five years of experience with needle interventions and four participants with a technical background and expertise in medical visualization.

The task was to insert a tracked needle from a predefined but unknown insertion path to a target point without using the MRI, relying only on the provided navigation clues. To this end, a phantom consisting of transparent candle wax gel with a slightly curved surface and inserted rubber o-rings of 2.3 cm in diameter was built (see Fig. 5). The rings served as targets and could easily be distinguished in the phantom's MRI dataset. The phantom surface was kept opaque by putting thin cardboard on it. This way, the users were not able to see the targets and had to rely only on the AR needle guidance clues. The cardboard also ensured that the needle would stay in place for measuring the accuracy achieved, which was done in a post-insertion MRI dataset. The process was repeated three times by each user. Fig. 5 and Fig. 6 show a user inserting the needle with the provided navigation clues into the phantom to the planned target point.

For this user study, the thresholds for the needle guidance color indicators were set very close to the target to achieve as accurate results as possible; e.g. the distance threshold to color the target green was 0.5 mm, the angle difference between needle and target was 0.5° . Because the success of an accurate insertion is clearly delimited by color changes, there should be no correlation between the duration of the puncture and the accuracy achieved.

Before the first trial, the users had the opportunity to practice insertion until they felt confident with the system. After each insertion, an MRI scan was carried out, the actual

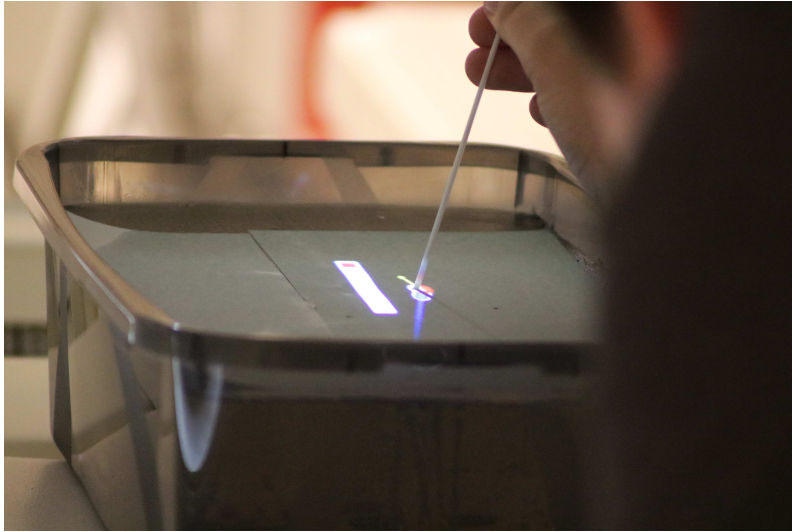


Figure 6: Same as Fig. 5, but from the view over the shoulder of the user. Virtual and real needle are accurately aligned for the users perspective in the middle of the MRI bore.

needle position was measured in the dataset, and the deviation to the planned path was calculated. The average positioning errors were calculated to serve as an accuracy indicator for the complete system, because all occurring calibration errors accumulate in them. After the insertion tests, an expert interview with the participants was carried out. The questions included advantages and drawbacks of the AR system and its suitability for the task.

4 Results

The AR system was assessed regarding its accuracy. The mean camera calibration reprojection error was 0.40 ± 0.19 px, that of the projector 0.62 ± 0.28 px, and that of the stereo calibration 0.94 ± 0.33 px. The repeated 100 pose estimations of the ChArUco markers used for the calibration revealed high repeatability with a standard deviation of only 0.1 mm in x direction, 0.2 mm in y direction and 0.7 mm in z direction at a distance of 650 mm, which is the distance between wide angle camera and the fixed MR marker. The Rodrigues angle axis only differed by (0.003;0.001;0.004) and a standard angle deviation of 0.003° .

In the following, the measured results of the user study are presented. All users finished training the navigated needle insertion after one test run. The overall difference between planned and real entry point was 1.7 ± 0.8 mm and the total target distance error was 1.7 ± 0.5 mm. The insertion took 102 ± 37 s. These values differ between the two user groups.

Compared to the overall performance, a slightly lower target distance error can be seen in the medical group than for the technical users (med: 1.5 ± 0.4 mm, tech: 1.8 ± 0.6 mm) in Fig. 7 at a similar insertion duration (med: 97 ± 41 s, tech: 107 ± 33 s). The technical users reached lower insertion point errors than the medical group (med: 2.0 ± 1.0 mm, tech: 1.4 ± 0.3 mm). No correlation between the insertion duration and the error of the entry point (PCC=-0.06) or the target distance error (PCC=0.22) could be found.

The answers of the users from the interviews were predominantly positive. All users agreed that the navigation clues in general helped them guide the needle from insertion point to the target in a clear and reliable way. All users perceived drops in the needle tracking speed especially before the insertion, caused by the distance to the MPT camera being too short, as a noticeable disadvantage. Full tracking speed was only reached at

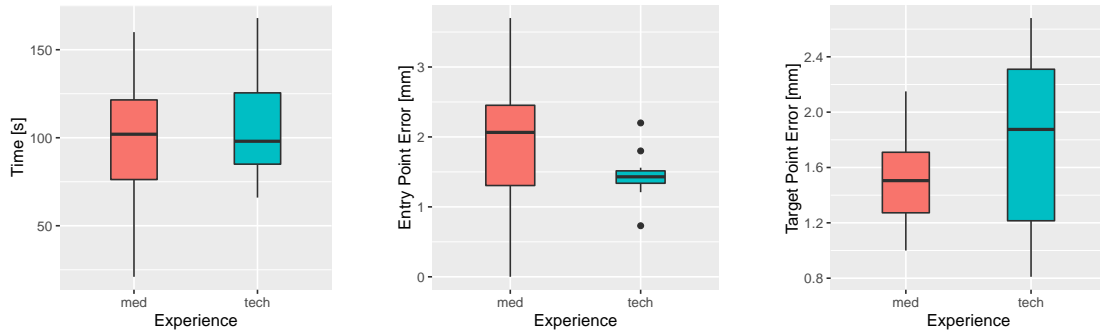


Figure 7: Boxplots for time, entry point error and target distance error grouped by experience (medical, technical).



Figure 8: Projection of a planned insertion point and contours of a rib on the non-flat surface of an abdomen phantom viewed from feet in the correct viewing position.

a distance of 25 cm from the camera. Some users of both groups highlighted a partial covering of the projection with the hand while guiding the needle, which could only be avoided by repositioning the hand.

The radiologists responded that the AR system is suitable for the insertion task. When asked about breathing motion correction, two of them stated that this is not a mandatory feature, because the insertion could be done in the seconds after exhalation, for which there already exists valid planning data. They also acknowledged that the field of dynamic registration and planning updates is complex and still the subject of extensive research. Some kinds of interventions, such as radio frequency ablation, could also be performed after completely immobilizing the patient. All medical participants agreed that the AR navigation system is a good support for MR-guided needle interventions, because the guidance allows for correctly oriented needle insertion for the important first stage during the insertion, so that fewer corrections are needed in deeper sections, which would injure more healthy tissue and move the target. Usage of the AR navigation alone was declined because of missing live updates, which can still be provided on the MRI scanner's interventional screen.

5 Discussion

We demonstrated an accurate projected AR system for intra-operative needle guidance on the patient phantom inside a wide-bore MRI. The quantitative measurements of planned and actual needle insertion points and target points, as well as their distances, serve as quality indicators of the preceding calibration and registration process. According to our clinical partners, the errors we achieved in this work for the entry point and for the target are sufficiently small for tumors with a size of 15 mm.

The authors are aware of the fact that the measurements from MRI datasets are inherently faulty due to the relatively low imaging resolution and the virtual malformation of the scanned object when processing the retrieved signals. The latter leads to straight lines appearing as curves. We attempted to preserve the validity of the 3D positions by using the built-in interpolation and distortion correction algorithms of the MRI. Because we did not move the test phantom during the study, all MRI scans yielded best possible reproducible results. Another error source is the stiffness of the applied needle. As the needle progressed deeper into the test phantom, it was deformed slightly, which led to a marginally different needle tip position than expected by the tracking system. This could be avoided by using a stiffer needle material. However, the results reflect the users' positive impressions of the AR needle guidance system. The projection was perceived to be in the correct perspective from the viewers' angle. The frame drops of the needle tracking rate were caused by the fixed focus plane being set too distant from the tracking camera. In the user study the needle had to be inserted mostly vertically, which represents the worst case in this regard. In clinical scenarios the needle is often inserted in a flatter angle and thus at a further distance, so that the full tracking speed can be exhausted. The ergonomics of this setup is assessed acceptable by the users, because the head does not need to be turned to an external monitor. This can prevent back and neck pain, but will need further long-term investigation.

Despite the promising accuracy assessment, the current AR needle guidance has some inherent limitations regarding interventions in real clinical scenarios. Because the needle guidance relies on non-real-time image data, the needle can only be inserted during respiratory arrest (passive or active), i.e. when the planning data matches the operating field. To react to changes of the projection surface due to breathing movements, especially for abdominal treatments, an approach to dynamically map the projection should be followed in further research, e.g. by using markers on the surface to track deformations [27].

More important than the skin movement is the deformation of organs and surrounding risk structures due to breathing. With additional live control imaging, this problem could be addressed. In further research, live 2D MRI images of the needle plane could be color corrected, projected onto, and aligned with the patient to give the radiologist the certainty of not damaging risk structures due to outdated imagedata. This is the primary reason why the authors decided to set up the needle guidance for in-bore usage instead of the in & out technique. Otherwise, the workflow would be disturbed by moving the patient into the MRI scanner for control imaging and back for needle placement. This way also all advantages of the MRI can be fully exhausted, i.e. morphological and functional imaging. An advanced method is the real-time fusion of ultrasound data with the MRI to compensate for organ motion [28, 29].

According to the feedback from the clinical users the AR system in its current state is already a valuable support for needle guidance, especially during the important first stage of the insertion, where the needle needs to be as accurately oriented as possible to prevent mandatory corrections later on. The projection interface should also be considered as an aid to convey the movements of the needle under the skin to improve the coordination of inexperienced radiologists.

6 Conclusion

For the first time, a projector-based AR system for use inside a wide-bore 3T MRI is introduced. We successfully set up a long-throw projector and a wide angle camera together with an optical moiré marker needle tracking system, calibrated the components, and registered them with the MRI. The calibration only has to be performed once when the hardware is set up. A fixed optical marker on the bottom of the bore provides persistence of the calibration. We also introduced a clear and robust visualization technique for needle guidance that is easy to understand, reliable and accurate.

In a user study with eight participants, four of whom were experienced radiologists, the overall accuracy was measured by inserting needles into a phantom using only the provided AR needle navigation system. The positioning errors were small but need to be evaluated further, e.g. with animal tests, to be able to make assumptions about the accuracy for patient use. At the current development stage and in a patient treatment scenario, the needle could be inserted during respiratory arrest or into organs that are not affected by breathing motion.

However, this prototype serves as a robust platform for further development, e.g. visualization techniques that improve depth perception, as proposed in Bork et al. [30], Hansen et al. [31] or Lawonn et al. [32], or are more robust against self-occlusion, e.g. with additional projectors. In addition, 2D MRI live images of the needle plane shall be aligned with the patient to enable uncomplicated and ergonomic access to control scans that are needed to overcome the limitations originating from breathing motion. To extend the support for risk visualization, an error cone as proposed in Alpers et al. [33] could be added to the scene. If applied as suggested, the proposed system has the potential to facilitate needle-based interventions inside closed-bore MRI scanners.

Funding

The work of this paper is partly funded by the Federal Ministry of Education and Research within the Forschungscampus *STIMULATE* under grant number 13GW0095A. The authors declare that they have no conflict of interest.

References

- [1] Buell Joseph F, Thomas Mark T, Rudich Steven, et al. Experience with more than 500 minimally invasive hepatic procedures *Annals of surgery*. 2008;248:475–486.
- [2] Schullian P., Widmann G., Lang T. B., Knoflach M., Bale R.. Accuracy and diagnostic yield of CT-guided stereotactic liver biopsy of primary and secondary liver tumors *Comput. Aided Surg.*. 2011;16:181–187.
- [3] Fischbach Frank, Bunke Jürgen, Thormann Markus, et al. MR-guided freehand biopsy of liver lesions with fast continuous imaging using a 1.0-T open MRI scanner: experience in 50 patients *Cardiovascular and interventional radiology*. 2011;34:188–192.
- [4] Kariniemi Juho, Sequeiros R Blanco, Ojala Risto, Tervonen Osmo. MRI-guided abdominal biopsy in a 0.23-T open-configuration MRI system *European radiology*. 2005;15:1256–1262.
- [5] Rempp Hansjörg, Loh Henning, Hoffmann Rüdiger, et al. Liver lesion conspicuity during real-time MR-guided radiofrequency applicator placement using spoiled gradient echo and balanced steady-state free precession imaging *Journal of Magnetic Resonance Imaging*. 2014;40:432–439.

- [6] Weiss Clifford R, Nour Sherif Gamal, Lewin Jonathan S. MR-guided biopsy: A review of current techniques and applications *Journal of Magnetic Resonance Imaging*. 2008;27:311–325.
- [7] Hoffmann Rüdiger, Thomas Christoph, Rempp Hansjörg, et al. Performing MR-guided biopsies in clinical routine: factors that influence accuracy and procedure time *European radiology*. 2012;22:663–671.
- [8] Bock Michael, Wacker Frank K. MR-guided intravascular interventions: Techniques and applications *Journal of Magnetic Resonance Imaging*. 2008;27:326–338.
- [9] Hillenbrand Claudia M, Elgort Daniel R, Wong Eddy Y, et al. Active device tracking and high-resolution intravascular MRI using a novel catheter-based, opposed-solenoid phased array coil *Magnetic resonance in medicine*. 2004;51:668–675.
- [10] Rothgang Eva, Gilson Wesley D, Wacker Frank, Hornegger Joachim, Lorenz Christine H, Weiss Clifford R. Rapid freehand MR-guided percutaneous needle interventions: An image-based approach to improve workflow and feasibility *Journal of Magnetic Resonance Imaging*. 2013;37:1202–1212.
- [11] Manzey D., Rottger S., Bahner-Heyne J. E., et al. Image-guided navigation: the surgeon’s perspective on performance consequences and human factors issues *Int J Med Robot*. 2009;5:297–308.
- [12] Gavaghan K, Oliveira-Santos Thiago, Peterhans Matthias, et al. Evaluation of a portable image overlay projector for the visualisation of surgical navigation data: phantom studies *International journal of computer assisted radiology and surgery*. 2012;7:547–556.
- [13] Gering David T, Nabavi Arya, Kikinis Ron, et al. An integrated visualization system for surgical planning and guidance using image fusion and an open MR *Journal of Magnetic Resonance Imaging*. 2001;13:967–975.
- [14] Wacker Frank K, Vogt Sebastian, Khamene Ali, et al. An Augmented Reality System for MR Image-guided Needle Biopsy: Initial Results in a Swine Model 1 *Radiology*. 2006;238:497–504.
- [15] Fichtinger Gabor, Deguet Anton, Masamune Ken, et al. Image overlay guidance for needle insertion in CT scanner *IEEE transactions on biomedical engineering*. 2005;52:1415–1424.
- [16] Weiss Clifford R, Marker David R, Fischer Gregory S, Fichtinger Gabor, Machado Antonio J, Carrino John A. Augmented reality visualization using image-overlay for MR-guided interventions: system description, feasibility, and initial evaluation in a spine phantom *American Journal of Roentgenology*. 2011;196:W305–W307.
- [17] U-Thainual P, Fritz Jan, Moonjaita Choladawan, et al. MR image overlay guidance: system evaluation for preclinical use *International journal of computer assisted radiology and surgery*. 2013;8:365–378.
- [18] Fritz Jan, U-Thainual Paweena, Ungi Tamas, et al. Augmented reality visualization with image overlay for MRI-guided intervention: accuracy for lumbar spinal procedures with a 1.5-T MRI system *American Journal of Roentgenology*. 2012;198:W266–W273.
- [19] Gavaghan K., Oliveira-Santos T., Peterhans M., et al. Evaluation of a portable image overlay projector for the visualisation of surgical navigation data: phantom studies *International Journal of Computer Assisted Radiology and Surgery*. 2012;7:547–556.

- [20] Gavaghan Kate Alicia, Anderegg Sylvain, Peterhans Matthias, Oliveira-Santos Thiago, Weber Stefan. Augmented reality image overlay projection for image guided open liver ablation of metastatic liver cancer in *Workshop on Augmented Environments for Computer-Assisted Interventions*:36–46Springer 2011.
- [21] Gavaghan Kate A, Peterhans Matthias, Oliveira-Santos Thiago, Weber Stefan. A portable image overlay projection device for computer-aided open liver surgery *IEEE Transactions on Biomedical Engineering*. 2011;58:1855–1864.
- [22] Sugimoto Maki, Yasuda Hideki, Koda Keiji, et al. Image overlay navigation by markerless surface registration in gastrointestinal, hepatobiliary and pancreatic surgery *Journal of hepato-biliary-pancreatic sciences*. 2010;17:629–636.
- [23] Besharati Tabrizi Leila, Mahvash Mehran. Augmented reality–guided neurosurgery: accuracy and intraoperative application of an image projection technique *Journal of neurosurgery*. 2015;123:206–211.
- [24] Moreno Daniel, Taubin Gabriel. Simple, accurate, and robust projector-camera calibration in *2012 Second International Conference on 3D Imaging, Modeling, Processing, Visualization & Transmission*:464–471IEEE 2012.
- [25] Garrido-Jurado S., Salinas R. Mu Madrid-Cuevas F.J., Marín-Jiménez M.J.. Automatic generation and detection of highly reliable fiducial markers under occlusion *Pattern Recognition*. 2014;47:2280 - 2292.
- [26] Garrido-Jurado S., Salinas R. Mu Madrid-Cuevas F.J., Medina-Carnicer R.. Generation of fiducial marker dictionaries using mixed integer linear programming *Pattern Recognition*. 2016;51:481 - 491.
- [27] Narita Gaku, Watanabe Yoshihiro, Ishikawa Masatoshi. Dynamic projection mapping onto deforming non-rigid surface using deformable dot cluster marker *IEEE transactions on visualization and computer graphics*. 2017;23:1235–1248.
- [28] Huang Xishi, Hill Nicholas A, Ren Jing, Guiraudon Gerard, Boughner Derek, Peters Terry M. Dynamic 3D ultrasound and MR image registration of the beating heart in *International Conference on Medical Image Computing and Computer-Assisted Intervention*:171–178Springer 2005.
- [29] Xu Sheng, Kruecker Jochen, Turkbey Baris, et al. Real-time MRI-TRUS fusion for guidance of targeted prostate biopsies *Computer Aided Surgery*. 2008;13:255–264.
- [30] Bork Felix, Fuers Bernhard, Schneider Anja-Katharina, Pinto Francisco, Graumann Christoph, Navab Nassir. Auditory and Visio-Temporal Distance Coding for 3-Dimensional Perception in Medical Augmented Reality in *Mixed and Augmented Reality (ISMAR), 2015 IEEE International Symposium on*:7–12IEEE 2015.
- [31] Hansen Christian, Wieferich Jan, Ritter Felix, Rieder Christian, Peitgen Heinz-Otto. Illustrative visualization of 3D planning models for augmented reality in liver surgery *International journal of computer assisted radiology and surgery*. 2010;5:133–141.
- [32] Lawonn Kai, Luz Maria, Hansen Christian. Improving spatial perception of vascular models using supporting anchors and illustrative visualization *Computers & Graphics*. 2017;63:37–49.
- [33] Alpers Julian, Hansen Christian, Ringe Kristina, Rieder Christian. CT-Based Navigation Guidance for Liver Tumor Ablation in *Eurographics Workshop on Visual Computing for Biology and Medicine*The Eurographics Association 2017.